J Electr Eng Technol Vol. 9, No. 3: 926-931, 2014
http://dx.doi.org/10.5370/JEET.2014.9.3.926

ISSN(Print) 1975-0102
ISSN(Online) 2093-7423

Parametric Analysis and Experimental Testing of Radial Flux Type Synchronous Permanent Magnet Coupling Based on Analytical Torque Calculations

Han-Bit Kang* and Jang-Young Choi†

Abstract – This paper presents the torque calculation and parametric analysis of synchronous permanent magnet couplings (SPMCs). Based on a magnetic vector potential, we obtained the analytical magnetic field solutions produced by permanent magnets (PMs). Then, the analytical solutions for a magnetic torque were obtained. All analytical results were extensively validated with the non-linear a two-dimensional (2D) finite element analysis (FEA). In particular, test results such as torque measurements are presented that confirm the analysis. Finally, using the derived analytical magnetic torque solutions, we carried out a parametric analysis to determine the influence of the design parameters on the SPMC's behavior.

Keywords: Synchronous permanent magnet couplings, Analytical magnetic field solutions, 2D FEA, Parametric analysis

1. Introduction

Synchronous permanent magnet couplings (SPMCs) are used to transmit torques between two rotating parts without mechanical contact. They are widely used in industrial applications e.g. ammonia pumps and centrifugal pumps for pharmaceutical and chemical industries. In particular, the coaxial type device is suitable for high torque demands. Knowledge regarding the SPMC pull-out torque is very important because this torque acts as an overload protection. Therefore, many researchers have performed torque analyses using finite element (FE) and other analytical methods.

Yonnet et al. [1] developed an analytical model to calculate the torque based on the exerted forces between bar-shaped magnets. Elies and Lemarquand [2] have shown that the optimization of coaxial SPMC using an analytical formula for the tangential force. Charpentier and Lemarquand [3] studied SPMCs with a Halbach magnetization using an analytical formulation. Ravaud et al. [4-5] showed a three-dimensional (3D) torque calculation for a radial magnetized SPMC and comparison of a radial and parallel magnetized permanent magnet (PM) for a single segment. Wu et al. [6] optimized the SPMC calculation using a 3D FE method. Wang et al. [7] determined the optimal design procedures of a radial model using the same method. Earlier studies usually used the radial magnetized PMs for the SPMC because radial magnetized PMs are good for obtaining a high torque, but they are difficult to manufacture. Therefore, this paper employs parallel magnetized PMs, which are easier to fabricate and cheaper than the radial type for SPMCs.

On the other hand, a magnetic field analysis is essential for predicting the torque. In order to accomplish this, the FE method is preferred. However, this method is often time-consuming and has poor flexibility. For this reason, this paper uses a parametric analysis based on analytical torque calculation and experimental testing of a radial flux type SPMC with parallel magnetized PMs. Based on the magnetic vector potential and two-dimensional (2D) polar coordinate system, we derived the analytical solutions for the magnetic fields produced by interaction between the leading and following PMs. Then, the magnetic torque was calculated using the magnetic field solutions and Maxwell stress tensor. The analytical results are in good agreement with those obtained from the FE analysis (FEA) and experimental results. Finally, based on analytical torque solutions, the influence of the various design parameters on the SPMC performances is investigated and discussed.

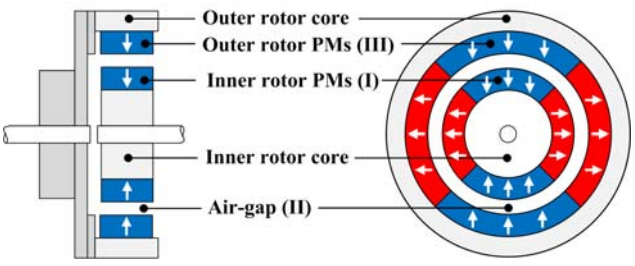

Fig. 1. SPMC structure with parallel magnetized PMs.

† Corresponding Author: Dept. of Electrical Engineering, Chungnam National University, Korea. (choi_jy@cnu.ac.kr)
* Dept. of Electrical Engineering, Chungnam National University, Korea. (kangbit@cnu.ac.kr)
Received: September 28, 2013; Accepted: December 28, 2013

2. Analysis of SPMC with Parallel Magnetized PMs

Fig. 1 shows the structure of a SPMC with parallel magnetized PMs. If the inner or outer rotor rotates, the other one follows due to the interaction between the inner and outer PMs. When a torque that exceeds the SPMC pull-out torque is applied, a slip occurs to protect the coupled machine or device from damage.

2.1 Analytical model of SPMC

Fig. 2 shows the analytical model of a SPMC that is composed of two polar coordinate systems: (r, α, z) axis for the outer rotor and (R, θ, Z) axis for the inner rotor. The gap between these axes is expressed as θ_a and represents the relative angular shift. The symbols *u, v, w,* and *x* represent the inner rotor internal and external radiuses, and outer rotor internal and external radiuses, respectively. In addition, α_p is the angular length of a pole and is expressed by the number of pole pairs (p): $\alpha_p = \pi / p$. The region is confined to 3 regions: (I) inner PMs, (II) air-gap, and (III) outer PMs. In addition, the assumptions for the analytical solutions are as follows:

- The permeability of the rotor cores is infinity;
- The permeability of the PMs is same as air.

The parallel magnetization model for a Fourier series expansion is shown in Fig. 3 [8]. The magnetization can be expressed as

$$\mathbf{M} = \sum_{n=-\infty,odd}^{\infty} \left(M_{rn} \cdot \mathbf{i_r} + M_{\theta n} \cdot \mathbf{i_\theta} \right) \cdot e^{-jnp(\alpha \text{ or } \theta)} \tag{1}$$

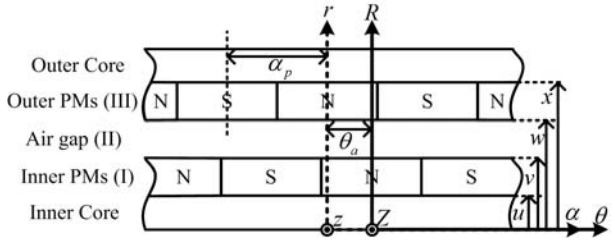

Fig. 2. Analytical model for the prediction of magnetic fields produced by PMs.

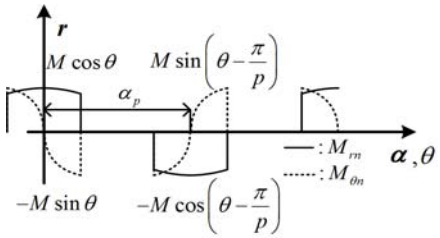

Fig. 3. Parallel magnetization model for a Fourier series expansion.

where n is the n^{th}-order space harmonic, $\mathbf{i_r}$ is the radial unit vector, and $\mathbf{i_\theta}$ is the circumferential unit vector. M_{rn} and $M_{\theta n}$ are the radial and circumferential Fourier coefficient components of magnetization, respectively.

2.2 Magnetic fields produced by parallel magnetized PMs

The magnetic flux density in the PM regions (I, III) can be expressed as $\mathbf{B} = \mu_0 (\mathbf{H} + \mathbf{M})$, where $\mu_0 = 4\pi \cdot 10^{-7}$ H/m and is the permeability of free space. Applying the curl operator to both sides of this equation yields

$$\nabla \times \mathbf{B} = \nabla \times \mu_0 \mathbf{M} \tag{2}$$

The magnetic field intensity (**H**) term is zero, $\nabla \times \mathbf{H} = \mathbf{J} = 0$, because there is no free current in this region. The magnetic flux density (**B**) can be represented using the magnetic vector potential (**A**), $\mathbf{B} \equiv \nabla \times \mathbf{A}$. Applying the curl operator to both sides of this equation and Coulomb gauge, $\nabla \cdot \mathbf{A} = 0$ leads to

$$\nabla \times B = -\nabla^2 A \tag{3}$$

Combining (2) and (3), yields the Poisson and Laplace equations in each region

$$\begin{aligned} \nabla^2 A^{I,III} &= -\mu_0 (\nabla \times M) \\ \nabla^2 A^{II} &= 0 \end{aligned} \tag{4}$$

The magnetic vector potential, **A,** can be written as

$$\begin{aligned} \mathbf{A^I} &= \sum_{n=-\infty,odd}^{\infty} A_n^I (r) \cdot e^{-jnp\theta} \cdot \mathbf{i_z} \\ \mathbf{A^{II}} &= \sum_{n=-\infty,odd}^{\infty} A_n^{II} (r) \cdot e^{-jnp\alpha} \cdot \mathbf{i_z} \\ \mathbf{A^{III}} &= \sum_{n=-\infty,odd}^{\infty} A_n^{III} (r) \cdot e^{-jnp\alpha} \cdot \mathbf{i_z} \end{aligned} \tag{5}$$

where $\mathbf{i_z}$ is the axial unit vector. Using (4) and (5), we can derive the magnetic vector potential as it relate to the magnetizations.

$$\begin{aligned} \mathbf{A^I} &= \sum_{n=-\infty,odd}^{\infty} \left\{ \begin{aligned} &C_n^I r^{np} + D_n^I r^{-np} \\ &+ \frac{\mu_0 (jnpM_{rn} + M_{\theta n})}{(np)^2 - 1} r \end{aligned} \right\} \cdot e^{-jnp\theta} \mathbf{i_z} \\ \mathbf{A^{II}} &= \sum_{n=-\infty,odd}^{\infty} \left\{ C_n^{II} r^{np} + D_n^{II} r^{-np} \right\} \cdot e^{-jnp\alpha} \mathbf{i_z} \\ \mathbf{A^{III}} &= \sum_{n=-\infty,odd}^{\infty} \left\{ \begin{aligned} &C_n^{III} r^{np} + D_n^{III} r^{-np} \\ &+ \frac{\mu_0 (jnpM_{rn} + M_{\theta n})}{(np)^2 - 1} r \end{aligned} \right\} \cdot e^{-jnp\alpha} \mathbf{i_z} \end{aligned} \tag{6}$$

The symbols C_n^I, C_n^{II}, C_n^{III}, D_n^I, D_n^{II}, and D_n^{III} are the coefficients. Using the definition of a magnetic vector potential, the magnetic flux density can be expressed as

$$\mathbf{B} = \sum_{n=-\infty,odd}^{\infty} \left\{ -\frac{jnp}{r} A_n(r) e^{-jnp(\alpha,\theta)} \mathbf{i}_r - \frac{\partial}{\partial r} A_n(r) e^{-jnp(\alpha,\theta)} \mathbf{i}_\theta \right\} \quad (7)$$

Finally, the magnetic flux density can be obtained in each region and direction as

$$\begin{aligned}
\mathbf{B}_r^I &= \sum_{n=-\infty,odd}^{\infty} -jnp \left(\begin{array}{l} C_n^I \cdot r^{np-1} + D_n^I \cdot r^{-np-1} \\ + \dfrac{\mu_0 \left(jnpM_{rn} + M_{\theta n} \right)}{(np)^2 - 1} \end{array} \right) \cdot e^{-jnp\theta} \cdot \mathbf{i}_r \\
\mathbf{B}_\theta^I &= \sum_{n=-\infty,odd}^{\infty} - \left(\begin{array}{l} C_n^I \cdot np \cdot r^{np-1} - D_n^I \cdot np \cdot r^{-np-1} \\ + \dfrac{\mu_0 \left(jnpM_{rn} + M_{\theta n} \right)}{(np)^2 - 1} \end{array} \right) \cdot e^{-jnp\theta} \cdot \mathbf{i}_\theta \\
\mathbf{B}_r^{II} &= \sum_{n=-\infty,odd}^{\infty} -jnp \left(C_n^{II} \cdot r^{np-1} + D_n^{II} \cdot r^{-np-1} \right) \cdot e^{-jnp\alpha} \cdot \mathbf{i}_r \\
\mathbf{B}_\theta^{II} &= \sum_{n=-\infty,odd}^{\infty} -\left(C_n^{II} \cdot np \cdot r^{np-1} - D_n^{II} \cdot np \cdot r^{-np-1} \right) \cdot e^{-jnp\alpha} \cdot \mathbf{i}_\theta \\
\mathbf{B}_r^{III} &= \sum_{n=-\infty,odd}^{\infty} -jnp \left(\begin{array}{l} C_n^{III} \cdot r^{np-1} + D_n^{III} \cdot r^{-np-1} \\ + \dfrac{\mu_0 \left(jnpM_{rn} + M_{\theta n} \right)}{(np)^2 - 1} \end{array} \right) \cdot e^{-jnp\alpha} \cdot \mathbf{i}_r \\
\mathbf{B}_\theta^{III} &= \sum_{n=-\infty,odd}^{\infty} - \left(\begin{array}{l} C_n^{III} \cdot np \cdot r^{np-1} - D_n^{III} \cdot np \cdot r^{-np-1} \\ + \dfrac{\mu_0 \left(jnpM_{rn} + M_{\theta n} \right)}{(np)^2 - 1} \end{array} \right) \cdot e^{-jnp\alpha} \cdot \mathbf{i}_\theta
\end{aligned} \quad (8)$$

The coefficients (C_n^I, C_n^{II}, C_n^{III}, D_n^I, D_n^{II}, D_n^{III}) in (8) can be derived from the proper boundary conditions and are given in the Appendix.

2.3 Magnetic torque

The interaction between the inner and outer PMs produces a force, F, which can be derived using the Maxwell Stress tensor [9]:

$$\begin{aligned}
\mathbf{F} &= -S\mu_0 \left\langle \mathbf{H}_r^{II}(w,\alpha) \mathbf{H}_\theta^{II}(w,\alpha) \right\rangle_\alpha \\
&= -\frac{S}{\mu_0} \left\{ \mathbf{B}_r^{II}(w,\alpha) \cdot \left(\mathbf{B}_\theta^{II}(w,\alpha) \right)^* \right\}
\end{aligned} \quad (9)$$

where the angle bracket expression $\langle\cdot\rangle_\alpha$ indicates the spatial average of the quantity enclosed by the brackets on α. The character, S, is the bottom surface of the outer PMs, which is expressed as $S=2\pi wl$ where l is the z-axis directional length of the PMs and the superscript * denotes the complex conjugate. Using this force, the magnetic torque T can be derived as $\mathbf{T} = w \times \mathbf{F}$.

3. Comparison of Analytical Predictions with Nonlinear FE Calculations and Measurements

For the parametric analysis, the validity of the analytical solutions must be confirmed using other methods such as numerical methods. To do this, 2D FEA and experiment are employed. For this stage, we manufactured a SPMC with parallel magnetized PMs that have the parameter values listed in Table 1. Figs. 4 (a) and (b) show the SPMC test apparatus for the pull-out torque measurements and a manufactured SPMC, respectively. Fig. 5 shows the magnetic field distributions obtained from the 2D FEA when θ_a is 0°, 45°, and 90°. The influence of the relative angular shift between inner and outer rotor on the magnetic field distributions can be determined using this technique.

Fig. 6 shows the comparison of the analytical calculations with the 2D FEA for the magnetic flux density when θ_a is (a) 0°, (b) 45°, and (c) 90° at $r = w$, and (d) produced torque. It can be observed that the magnetic field distribution and torque vary with the angular position. The analytical results are in good agreement with the 2D FEA. Table 2 shows the comparison between the analytical and measured results for the pull-out torque of the SPMC. As expected, the analytical torque results are in good agreement with the measured results. The error seems to be

Table 1. Design parameters of the manufactured SPMC with parallel magnetized PMs.

Parameter	Value	Parameter	Value
u	12 mm	Pole arc ratio	1
v	20 mm	Pole-pairs	2
w	27 mm	z-directional length	40 mm
x	35 mm	Shaft radius	7 mm

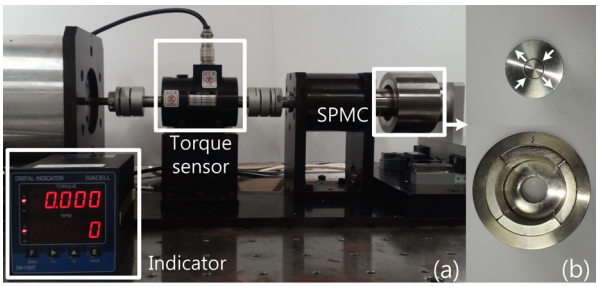

Fig. 4. Photograph of the (a) test apparatus for the torque measurements and (b) manufactured SPMC.

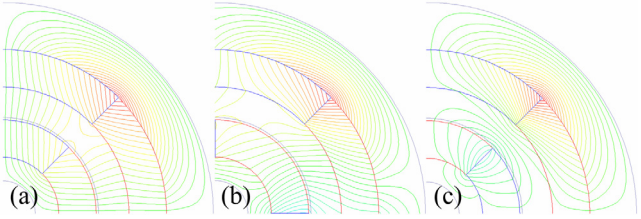

Fig. 5. Magnetic field distribution from a 2D FEA when θ_a is (a) 0°, (b) 45°, and (c) 90°.

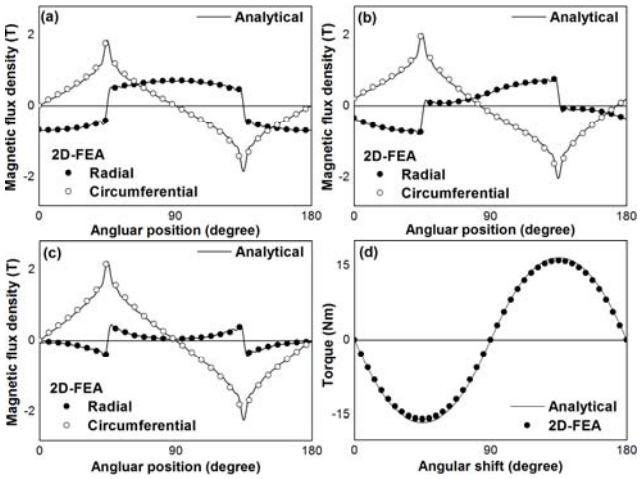

Fig. 6. Comparison between the analytical predictions and 2D FEA results for the magnetic flux density when θ_a is (a) 0°; (b) 45°; (c) 90° at the air gap, and (d) the produced torque.

Table 2. Comparison between the analytical and measured results for the pull-out torque of the SPMC.

Measurement	2-D FEA result (Error)	Analytical result (Error)
15.051	15.9211 (5.78 %)	16.5087 (9.69 %)

Table 3. Initial value of design parameters used for the parametric analysis.

Parameter	Values
PM thickness	5 mm
Air gap length	2 mm
Pole arc ratio	1
PM thickness ratio	1

caused by leakage flux and manufacturing process error.

4. Parametric Analysis

The analytical torque solutions were used to investigate the influence of the design parameters on SPMC torque. The initial parameter values are listed in Table 3. Here, PM thickness ratio is defined as the inner PM thickness divided by the outer PM thickness.

4.1 PM thickness

It should be noted that the parameters listed in Table 3 are fixed to investigate the influence of the PM thickness on the magnetic torque. The variations of magnetic torque with respect to the PM thickness are predicted and shown in Fig. 7 (a) for various number of pole-pairs. It can be observed for each pole-pairs number that the pull-out torque increases, as the PM thickness increases. However, it is interesting that for each PM thickness, the torque of

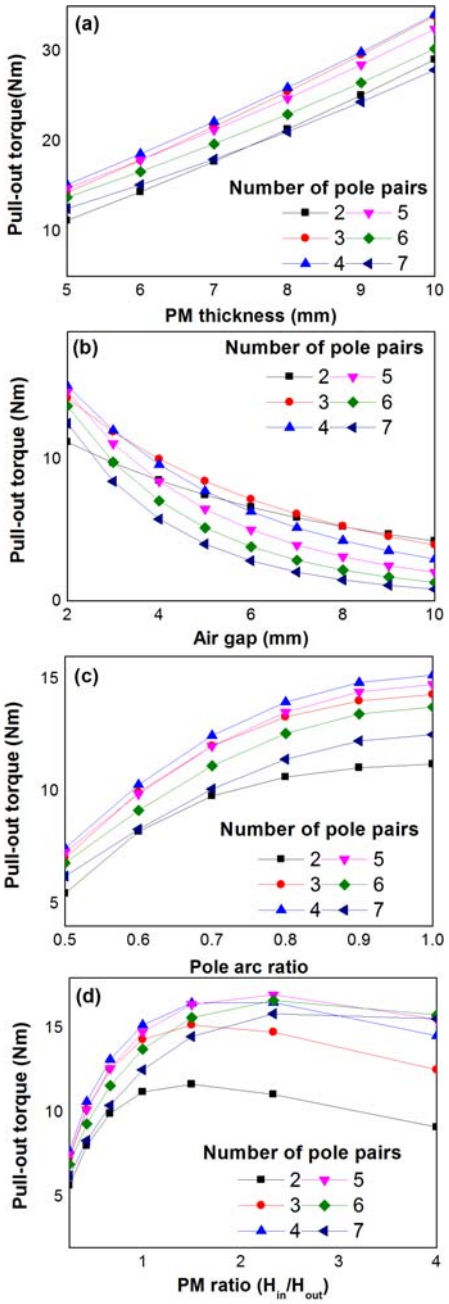

Fig. 7. Variation of pull-out torque according to (a) PM thickness; (b) air gap; (c) pole arc ratio, and (d) PM thickness ratio.

the 4 pole-pairs model is larger than the 5, 6, and 7 pole-pairs model.

4.2 Air gap length

All the parameters except for the air gap length and number of pole pairs were fixed. The variations in the calculated magnetic torque with respect to the air gap length for various numbers of pole-pairs are shown in Fig. 7 (b). It was observed that for each pole-pair number, the pull-out torque decreases, as the air-gap length increases.

In particular, the 2 pole-pairs model has smaller torque sensitivity according to air gap length than the other models.

4.3 Pole arc ratio

In this section, all the parameters are fixed except for the pole arc ratio and number of pole pairs. The variations in the calculated magnetic torque with respect to the pole arc ratio for various numbers of pole-pairs are shown in Fig. 7 (c). It can be seen that the pull-out torque is greatly increases with respect to the pole arc ratio especially in the range of 0.5 and 0.8. When the pole arc ratio is greater than 0.8, the increase in torque is not as significant.

4.4 PM thickness ratio

Here, the air gap length and pole arc ratio values are fixed. The variations between the calculated magnetic torque with respect to the PM thickness ratio for various numbers of pole-pairs are shown in Fig. 7 (d). It can be observed that the optimal ratio is directly proportional to the number of pole pairs. In addition, if the SPMC is manufactured with a 1 pole arc ratio, the 4 pole-pairs model is dominant.

5. Conclusions

Analytical magnetic field calculation techniques for a SPMC have been developed. Based on the magnetic vector potential and 2D polar coordinate system, the analytical solutions for a magnetic field produced by PMs have been presented. In addition, the magnetic torque has been calculated using the magnetic field solutions and Maxwell stress tensor. The predicted pull-out torque results are in good agreement with the nonlinear FEA results and measurements. Finally, the influence of various design parameters on the performance of the SPMCs has been investigated using torque calculations. The analytical method proposed here should be very useful in initial design and optimization process of SPMCs with parallel magnetized PMs.

Appendix

The coefficients in (8) are expressed as follows:

$$
\begin{aligned}
C_n^I &= C_n^{II} \cdot e_1 - y_2 \\
C_n^{II} &= C_n^{III} + y_4 \\
C_n^{III} &= D_n^{III} \cdot x^{-2np} - y_6 \\
D_n^I &= D_n^{II} \cdot e_1 + y_3 \\
D_n^{II} &= D_n^{III} + y_5 \\
D_n^{III} &= \frac{y_6 + z_2}{x^{-2np} - u^{-2np}}
\end{aligned}
$$

where, ω_r is the rotating angular speed and

$$
\begin{aligned}
x_1 &= \frac{\mu_0 (jnpM_{rn} + M_{\theta n})}{(np)^2 - 1} \\
e_1 &= e^{jnp\omega_r t} \\
y_1 &= \frac{u^{-np+1}}{np}\left(\mu_0 M_{\theta n} + x_1\right) \\
y_2 &= \frac{v^{-np+1}}{2np}\left(\mu_0 M_{\theta n} + x_1 + npx_1\right) \\
y_3 &= \frac{v^{np+1}}{2np}\left(\mu_0 M_{\theta n} + x_1 - npx_1\right) \\
y_4 &= \frac{w^{-np+1}}{2np}\left(\mu_0 M_{\theta n} + x_1 + npx_1\right) \\
y_5 &= -\frac{w^{np+1}}{2np}\left(\mu_0 M_{\theta n} + x_1 - npx_1\right) \\
y_6 &= \frac{x^{-np+1}}{np}\left(\mu_0 M_{\theta n} + x_1\right) \\
z_1 &= \frac{1}{e_1}\left(-y_1 + y_2 + y_3 \cdot u^{-2np}\right) \\
z_2 &= y_5 \cdot u^{-2np} - y_4 + z_1
\end{aligned}
$$

Acknowledgements

The present work is a result of the project "Development of the design technologies for a 10MW class wave and offshore wind hybrid power generation system and establishment of the sea test infra-structure" granted by the Ministry of Oceans and Fisheries. All support is gratefully acknowledged.

References

[1] JP. Yonnet, S. Hemmerlin, E. Rulliere, and G. Lemarquand, "Analytical calculation of permanent magnet couplings," *IEEE Trans. Magnetics*, vol.29, no.6, pp.2932-2934, Nov. 1993.

[2] P. Elies and G. Lemarquand, "Analytical Optimization of the Torque of a Permanent-Magnet Coaxial Synchronous Coupling," *IEEE Trans. Magnetics*, vol. 34, no. 4, pp. 2267-2273, Jul. 1998.

[3] J.F. Charpentier and G. Lemarquand, "Study of Permanent-Magnet Couplings with Progressive Magnetization Using an Analytical Formulation," *IEEE Trans. Magnetics*, vol.35, no.5, pp.4206-4217, Sep. 1999.

[4] R. Ravaud, G. Lemarquand, V. Lemarquand, and C. Depollier, "Permanent Magent Couplings: Field and

Torque Three-Dimensional Expressions Based on the Coulombian Model," *IEEE Trans. Magnetics*, vol. 45, no. 4, Apr. 2009.

[5] R. Ravaud, G. Lemarquand, V. Lemarquand, and C. Depollier, "Torque in permanent magnet couplings: Comparison of uniform and radial magnetization," *Journal of Applied Physics*, vol. 105, issue. 5, Mar. 2009.

[6] W. Wu, H. C. Lovatt, J. B. Dunlop, "Analysis and Design Optimisation of Magnetic Couplings Using 3D Finite Elemet Modelling," *IEEE Trans. Magnetics,* vol.33, no.5, Sep. 1997.

[7] Wang Yu Lin, Liu Pin Kuan, Wu Jun, and Ding Han, "Near-Optimal Design and 3-D Finite Element Analysis of Multiple Sets of Radial Magnetic Couplings," *IEEE Trans. Magnetics,* vol. 44, no. 12, Dec. 2008.

[8] Zhu, Z.Q., Howe, D. and Chan, C.C., "Improved analytical model for predicting the magnetic field distribution in brushless permanent-magnet machines", *IEEE Trans. Magn.*, vol. 38, pp. 229-238, Jan. 2002.

[9] David L. Trumper, Won-jong Kim, and Mark E. Williams, "Design and Analysis Framework for Linear Permanent-Magnet Machines", *IEEE Trans. IAS,* vol. 32, pp. 371-379, 1996.

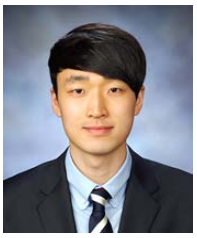

Han-Bit Kang He received B.S. degree in electrical engineering from Chungnam National University in 2013. His research interests are synchronous permanent magnet coupling, linear generator for wave energy converter.

Jang-Young Choi He received his B.S., M.S., and Ph.D. degrees from Chungnam National University in 2003, 2005, and 2009, respectively. In 2009, he worked as a researcher in Halla Climate Control Corporation. August 2009, Dr. Choi joined as an assistant professor the Department of Electrical Engineer-ing at Chungnam National University, Daejeon, Korea. His interests are in the design, analysis, simulation, and implementation of linear and rotary motors and permanent magnet generators.